Interdisciplinary Research in Medical Sciences Specialty
ISSN: 3062-4401
2021, Volume 1, Issue 1, Page No: 62-78

Available online at: www.galaxypub.co/page/journals

Galaxy Publication

Galaxy Publication

Modeling Hospital Patient Flow as an Interconnected Compartmental System: Equilibrium and Stability Analysis

David Miller[1], Eric Johnson[1], Matthew Clark[1], Steven Anderson[1]*

[1]Department of Biomedical Engineering, Faculty of Engineering, Stanford University, Stanford, USA.

***E-mail** ✉ steven.anderson.lab@gmail.com

Received: 26 January 2021; **Revised:** 11 March 2021; **Accepted:** 11 March 2021

ABSTRACT

Efficiently directing patient movement within hospitals is essential for delivering effective secondary care. By treating a hospital as a set of linked compartments through which patients transition, we formulate equations that describe these flows as a network of interdependent dynamic processes. Many influences shape these interactions—some identifiable, many interacting in complex ways. Unlike discrete-event or agent-based methods, this approach does not require detailed knowledge of every underlying factor; instead, it focuses on the overall transfers between units, consistent with a system-dynamics framework. Using this perspective, we identify two equilibrium conditions: a trivial state in which no patients are present, and a non-trivial state representing ongoing activity. We intend to analyse bed-occupancy data from a UK hospital to test the validity of this approach and evaluate how widely it can be applied.

Keywords: Dynamics, Bed-usage modelling, Stability assessment, Bifurcation evaluation

How to Cite This Article: Miller D, Johnson E, Clark M, Anderson S. Modeling Hospital Patient Flow as an Interconnected Compartmental System: Equilibrium and Stability Analysis. Interdiscip Res Med Sci Spec. 2021;1(1):62-78. https://doi.org/10.51847/oaa1Oz7Voc

Introduction

The National Health Service (NHS) in the United Kingdom is under significant strain, particularly regarding the availability of hospital beds. A key contributor to challenges in secondary (hospital) care is that the UK maintains one of the lowest counts of hospital beds per capita among OECD nations [1]. Consequently, managing the progression of patients through hospitals has become increasingly difficult. The combined effect of limited capacity and growing demand led to bed-occupancy figures rising from 87.7% in quarter 3 of 2010/11 to 92% in Q3 of 2019/20—just before the pandemic [2].

As secondary care grows more complicated, bed numbers often emerge as the main constraint on service delivery. Improving the effectiveness of bed utilization (and reducing associated opportunity costs) is therefore crucial for decision-makers. Although numerous attempts have been made to model bed use within specific departments (micro-level) or across broader healthcare systems (macro-level), only a small number of models provide a dependable, whole-hospital representation that follows patients from admission through discharge or death while accounting for interactions among clinical areas. Individuals with serious conditions (such as COVID-19, hereafter *Covid*) enter, move through, and exit hospitals. By regarding the hospital as a system composed of several compartments, our aim is to derive equations describing how these areas interact dynamically. These interconnections depend on many variables—some measurable, others mutually dependent. The central research question here is: How can a dynamical-systems framework be used to represent patient transitions across hospital departments so as to enhance bed utilization and inform resource planning? The motivation for this work stems from the fact that existing frameworks frequently concentrate on particular units or narrow situations (for instance, emergency departments or Covid-related flows) and thus fail to portray the hospital-wide dynamics that shape overall capacity.

We cannot, and need not, identify every driver influencing these flows—as required in discrete-event or agent-based approaches—and instead attend to the aggregate movements between compartments, consistent with a system-dynamics methodology.

Background

Given sustained pressure on bed availability, hospital administrators continually look for strategies that improve their use. Doing so requires understanding the principal patient groups and the way they progress through the system. More than fifty years ago, mathematical modelling was proposed as a means of supporting improved bed management [3]. A variety of deterministic, stochastic, multistage, and algorithmic techniques have since been applied, each with limitations. Examples include: concentrating on elective admissions [4, 5]; restricting analysis to a single, often highly specialized, ward [6–10]; addressing only part of the clinical workload without defining patient categories [11]; or focusing on medium-term capacity planning for an entire hospital [12] or an urban health network [13, 14]. Among the more comprehensive attempts was StratBAM [15], developed for a U.S. hospital equipped with complete electronic records—conditions that differ markedly from NHS settings. The lone systematic review of simulation models in this domain examined patient flow specifically within UK emergency departments [8], and even within that narrow focus, the evidence base was described as "small and poorly developed."

The *Covid* pandemic magnified these pressures worldwide, inspiring numerous investigations aimed at predicting bed requirements. Although these studies varied in scope, most did not address all general medical admissions (Covid and non-Covid) within a single hospital. A systematic review on surge-capacity planning identified 690 publications, but only six models capable of projecting both case volumes and capacity needs over time [16]. None investigated patient-movement patterns inside hospitals. Other research concentrated solely on Covid-related resource requirements (primarily to guide the use of limited intensive-care capacity) [17], or explored hospital-bed efficiency at a national scale [18], or examined planning for new-bed construction [19].

General model and description

To explore how delays in admission queues might influence mortality, we outline the connections among the compartments shown in **Figure 1** as follows:

Direct effects

There is strong observational support for the relevance of:

• The volume of beds allocated to and occupied by medical patients, as opposed to those used by other specialties—such as surgery, orthopaedics, gynaecology, and so on (as previously noted), and

• The daily total of patients taken on by the medical on-call team within a 24-hour window. Individuals admitted under the medical service typically represent a reasonably consistent mixture of conditions (e.g., myocardial infarction, stroke, diabetic complications, infections). Although this distribution shifts across days and seasons, it tends to remain quite steady across longer timescales (year-to-year). It is also well documented that emergency-admission numbers vary with the day of the week, with weekdays showing more than double the volume of weekend admissions.

Indirect effects

Reduced throughput in the ED may reflect wider cultural or resource-related issues. For instance, weaknesses in local organisational leadership might impede performance across multiple departments. Likewise, difficulties within regional social-care services may delay transfers of patients who are medically fit for discharge, affecting all wards—including the ED (i.e., vectors 1–4 in **(Figure 1)**)—a pattern currently common across many NHS hospitals.

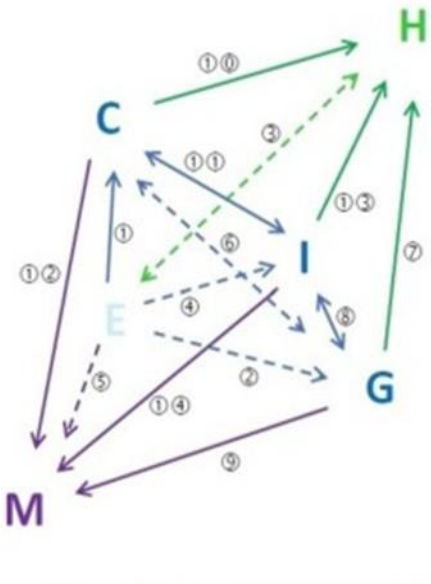

node	item
E	ED
G	General ward
C	COVID ward
I	ICU
H	Home
M	Mortuary

#	edge
1	E—C
2	E—G
3	E—H
4	E—I
5	E—M
6	G—C
7	G—H
8	G—I
9	G—M
10	C—H
11	C—I
12	C—M
13	I—H
14	I—M

Figure 1. This schematic illustrates the dynamic balance among hospital units, beginning with entry through the emergency department (E), progressing through the wards (G, C, I), and ending in discharge (H) or death (M).

During the pandemic period (up to March 2024), the weekly number of hospitalised Covid patients in England ranged from 45 to 3800. Across 2020–2021, emergency medical admissions averaged roughly 7,300, and during the largest wave of Covid infections, the doubling time for admissions in early March was 26 days, while the halving time in April was 20 days. Admission numbers are highly dependent on the quantity of unoccupied beds on a given day (as admitting thresholds are adjusted accordingly). The proportion of Covid admissions naturally tracks the prevailing level of community transmission. We assume that knowing the current hospital census and available capacity enables estimation of the number of patients who will require critical-care support (i.e., ICU beds) over the next 24 hours. Since shifts in non-epidemic case mix occur over months to years, whereas epidemic dynamics evolve within days—and because our focus is a 24-hour timescale—we treat non-epidemic case mix as effectively constant. The components of the model are summarised in **Figure 1**, and can be expressed in Eq. (1) as follows:

$$\begin{aligned}
\frac{dE}{dt} &= F_1(E,C) = rE\left(1-\frac{E}{K}\right) - \frac{aEC}{1+b_1E},\\
\frac{dC}{dt} &= F_2(E,C,G,I) = \frac{\Gamma_1 aEC}{1+b_1E} - m_1C - \frac{\beta GC}{1+b_2C}\left(1+\frac{\zeta I}{1+\epsilon I}\right),\\
\frac{dG}{dt} &= F_3(C,G,I) = \frac{\Gamma_2 \beta IC}{1+b_2C}\left(1+\frac{\zeta I}{1+\epsilon I}\right) - m_2G,\\
\frac{dI}{dt} &= F_4(E,C,I) = \frac{\beta aEC}{1+b_1E} - m_3I + \omega E.
\end{aligned} \tag{1}$$

Here Fi, i=1,2,3,4 denotes the interaction terms that shape the behaviour of the model. The endogenous (dependent) variables are defined as follows:

- E – population in the emergency department
- C – occupancy of the specialist ward(s) (in this context, the Covid ward)
- G – number of patients in the general medical ward
- I – ICU population
- H – individuals at home (represented implicitly through the ωE component)
- m – mortality

The initial conditions for the system in Eq. (1) are set so that $(0)\geq 0$, $C(0)\geq 0$, $G(0)\geq 0$, and $I(0)\geq 0$. The model outlines how patients enter the ED, a process driven both by infection prevalence and by hospital outflow (discharges plus deaths) once Covid pressure subsides. The parameter r captures admission volume, a represents

the rate at which patients are processed from the ED to the Covid ward (C), and when infection levels are low, a functions as a half-saturation constant. The quantity β specifies the linear flow into the ICU (I). The parameters Γi i=1,2, describe transitions between E and the other departments. The symbol ζ reflects day-to-day variation in virus transmission within the ED population. The parameter ϵ is central to simplifying the full four-compartment framework into a reduced special-case model. Mortality parameters Mi,=1,2,3 give the death rates, while ω In Eq. (1), the first component uses a logistic structure to describe daily hospital activity. Here, K represents total hospital capacity, and rE includes all medical admissions—heart attacks, strokes, sepsis, seizures, diabetic complications, etc.—whose long-term proportions remain comparatively stable. The combined recruitment rate of susceptible patients and natural mortality is expressed as $\alpha=r-d$. The total in-hospital population is summarised as $E=C+G+I$, where C corresponds to the Covid ward, G to the general medical ward, and I to the ICU. Although the hospital could be expressed with seven separate compartmental equations, the framework here is condensed into four. The second component of the first equation applies a Holling type II response to describe transfers from admission (E) to the Covid department (C).

The confirmed infected population in I (the ICU) can also be represented using a Holling type II response. Here, $\Gamma 1$ acts as the transition parameter governing movement from C to I. Mortality M appears in the second, third, and fourth equations of Eq. (1), reflecting deaths in multiple departments. In reality, these rates depend on factors such as recovery times, the number of infectious patients requiring care, and bed occupancy during peak demand. The third term introduces additional mortality, with βC quantifying Covid-related effects on ICU patients; the infected population in ICU can reach a saturation level adjusted by the factor $(1+\epsilon C)$. The second and third equations in the system describe patient movement from C to G using a Holling type II term with parameter a which reflects transfer time between departments.

The final equation represents the main hospital pathway during Covid conditions. The first term captures patient movement between the ICU and rehabilitation units, with E denoting ED inflow, ω representing the recovery or discharge rate, and M denoting daily mortality. Any hospital contains at least seven functional compartments, and movement across them is influenced by several factors, including:

- Administrative workflow and service quality, represented through the logistic component in Eq. (1).
- Workforce capacity—affected by issues such as staff illness—embedded in the resource parameter K.
- Severity of illness or infection in Covid cases, modelled in the second equation of Eq. (1).
- Ward-specific capacity (beds and space), reflected in the third and final equation of Eq. (1).

Analysis of the model equilibrium

This section gives a detailed examination of the system's behaviour and the equilibrium structure derived from Eq. (1). We produce explicit analytical forms for locating equilibria and for determining their stability under general parameter choices, and then evaluate outcomes for the specific cases K=500 and K=100. The following section broadens this to the entire interval $0\leq K\leq 1000$.

Location of equilibria

The equilibrium configurations $E(t)=Ee$, $C(t)=Ce$, $G(t)=Ge$ and $I(t)=Ie$ f Eq. (1) arise when $dE/dt=dC/dt=dG/dt=dI/dt=0$. A steady state for the autonomous system $y'=(y)$ is understood as any point $y0$ with the property that for every $\epsilon>0$, one can choose a $\delta>0$ such that any solution $\psi(t)$ of $y'=f(y)$ satisfying $\|\psi(t)-y0\|<\delta$ remains within ϵ of $y0$ for all $t\geq t0$. In other words, stability requires the existence of some $\delta 0>0$ such that if $\|\psi(t0)-y0\|<\delta 0$, then $\lim t\to+\infty\psi(t)=y0$. Applying this criterion to the system in Eq. (1) yields five candidate equilibrium points, listed in **Table 1**, corresponding to the four steady-state values (Ee,Ce,Ge,Ie) produced by the model.

- The third equilibrium, although mathematically acceptable, has no clinical relevance.

$$E_3 = \left(0, \frac{m_2}{\beta\Gamma_2 - b_2 m_2}, \frac{-m_1\Gamma_1}{\beta\Gamma_2 - b_2 m_2}, 0\right) \tag{2}$$

- The fourth equilibrium, representing the state in which the general medical ward is unoccupied, is expressed as follows:

$$E_4 = (E, C, 0, I), \tag{3}$$

$$E = \frac{1}{a\Gamma_1 - b_1 m_1}\frac{m_2}{\beta\Gamma_2 - b_2 m_2}, C = \frac{r\Gamma 1(ak\Gamma 1 - kb1m1 - m1)}{k(a\Gamma_1 - b_1 m_1)^2},$$
$$G = 0,$$
$$I = \frac{m_1(a\beta kr\Gamma_1 - \beta krb_1 m_1 + ak\omega\Gamma_1 - k\omega b_1 m_1 - \beta r m_1)}{k m_3 (a\Gamma_1 - b_1 m_1)^2}.$$

• The fifth, representing the complete dynamical equilibrium, corresponds to the full persistence regime and is determined by a quartic polynomial of the form shown below:

$$\sum_{i=0}^{4} A_i E_e^{4-i} = 0, (4) \quad (4)$$

where Ai, i=0,..,4 are the hierarchical parameters.

Table 1. Candidate equilibria of the system in Eq. (1), including both clinically relevant and irrelevant cases.

Equilibrium	Definition	Value in a parametrized system	Description
E_1	(E_e, C_e, G_e, I_e)	(0, 0, 0, 0)	Trivial equilibrium (empty hospital)
E_2	(E_e, C_e, G_e, I_e)	(K, 0, 0, Kω_{m3})	Equilibrium with full hospital resources and active ICU only
E_3	(E_e, C_e, G_e, I_e)	(0, C, −G, 0)	Clinically irrelevant (non-physical) point given in Eq. (2)
E_4	(E_e, C_e, G_e, I_e)	(E, C, 0, I)	General medical ward-free equilibrium given by Eq. (3)
E_5	(E_e, C_e, G_e, I_e)	(E, C, G, I)	Full dynamical (endemic) equilibrium given in Eq. (4)

Qualitative analysis of equilibrium positions

The Jacobian matrix for the four-compartment model is expressed as follows:

$$J = \begin{bmatrix} a_{11} & a_{12} & a_{13} & a_{14} \\ a_{21} & a_{22} & a_{23} & a_{24} \\ a_{31} & a_{32} & a_{33} & a_{34} \\ a_{41} & a_{42} & a_{43} & a_{44} \end{bmatrix},$$

Here, aij, with i,=1,...,4, denote the partial derivatives comprising the Jacobian matrix. The stability of the four equilibrium points is assessed through the eigenvalues of this matrix. In the next section, we examine the dynamics associated with each equilibrium.

$$a_{1,1} = \frac{-2E^3 rb_1^2 - E^2(krb_1^2 + 4rb_1) - 2E(krb_1 + r) - kr + aCk + 2\}}{k(Eb_1 + 1)^2}$$
$$a_{1,2} = -\frac{aE}{(Eb_1 + 1)}$$
$$a_{1,3} = 0,\ a_{1,4} = 0$$
$$a_{2,1} = \frac{\Gamma_1 aC(1 + b_1 E) - \Gamma_1 aEC \cdot b_1}{(1 + b_1 E)^2}$$
$$a_{2,2} = \frac{\Gamma_1 aEC}{1 + b_1 E} - m_1 C - \frac{\beta G(1 + b_2 C) - \beta GC \cdot b_2}{(1 + b_2 C)^2}(1 + \frac{\zeta I}{1 + \epsilon I})$$
$$a_{2,3} = -\frac{\beta C}{Cb_2 + 1} + \frac{\beta C(\zeta) I}{(1 + I)(Cb_2 +)}$$
$$a_{2,4} = \frac{\beta GC\zeta}{(1 + I)^2(Cb_2 + 1)}$$
$$a_{3,1} = 0$$
$$a_{3,2} = \frac{\Gamma_1 aEC}{1 + b_1 E} - m_1 C - \frac{\beta G(1 + b_2 C) - \beta GC \cdot b_2}{(1 + b_2 C)^2}(1 + \frac{\zeta I}{1 + \epsilon I})$$
$$a3,3 = -m2$$
$$a_{3,4} = \frac{\Gamma_2 \beta C(1 + b_2 C) - \Gamma_2 \beta IC \cdot b_2}{(1 + b^2 C)^2} \cdot \frac{\zeta(1 + \epsilon I) - \zeta I \cdot \epsilon}{(1 + \epsilon I)^2}$$

$$a_{4,1} = \frac{\beta aC}{Eb_1 + 1} - \frac{\beta aECb_1}{(Eb_1+)^2} + \omega$$
$$a_{4,2} = \frac{\beta aE}{Eb_1 + 1}$$
$$a4,3 = 0$$
$$a_{4,4} = -m_3$$

System behaviour near the origin E1

A simple analysis indicates that the hyperbolic, or first trivial, equilibrium functions as a stable fixed point.

$$\lambda_{E1} = (-r, m_1, m_2, m_3) \tag{5}$$

System behaviour near the hospital capacity and ICU equilibrium E2E

Evaluating the Jacobian of the system in Eq. (1) at the non-feasible point $E2=(K,0,0,\frac{K\omega}{M3})$ yields the following eigenvalues.

$$\lambda_1 = -r, \quad \lambda_2 = \frac{ak\Gamma_1 - kb_1m_1 - m_1}{kb_1 + 1}, \quad \lambda_3 = -m_2, \quad \lambda_4 = -m_3 \tag{6}$$

This equilibrium represents a saddle-type configuration. Three of the eigenvalues are negative, showing that perturbations along these directions will diminish over time, causing trajectories to return toward the equilibrium. The remaining positive eigenvalue indicates an unstable direction, where small deviations amplify, moving the system away from the point. Thus, a saddle point is defined by having a mix of stable and unstable directions.

System behaviour near the clinically irrelevant point E3 in Eq. (2)

For the non-feasible point $E3=(0,C,-G,0)$, the Jacobian matrix of Eq. (1) produces eigenvalues that describe the local dynamics around this equilibrium.

$$\lambda_1 = -\frac{-\beta r\Gamma_2 + rb_2m_2 + am_2}{\beta\Gamma_2 - b_2m_2} \tag{7}$$

where $\lambda 2,3$ is given in Eq (8) as follows:

$$\lambda_{2,3} = \pm\frac{1}{2}\frac{-m_1m_2b_2 + \sqrt{4\beta^2\Gamma_2^2m_1m_2 - 4\beta\Gamma_2b_2m_1m_2^2 + b_2^2m_1^2m_2^2}}{\beta\Gamma_2} \tag{8}$$

$$\lambda_4 = -m_3 \tag{9}$$

The point of equilibrium is classified as a saddle-focus, combining regions of stability and instability with inherent oscillations. Real eigenvalues primarily dictate stability, whereas the oscillatory behavior originates from complex conjugate eigenvalues.

The behavior of the system near the free equilibrium of the general medical ward, $E4$, can be expressed using Eq. (3).

For the fourth equilibrium in Eq. (1), where the general medical ward has no occupants (G=0), the corresponding Jacobian matrix is defined as follows.

$$\lambda_1 = \frac{-\alpha}{\beta} \tag{10}$$

Here, α and β represent two sequentially dependent parameters, as defined in Eq. (23) and Eq. (24).

$$\lambda_{2,3} = \pm\frac{(a\Gamma_1 - b_1m_1)}{2ak\Gamma 1} \sqrt{a^2k\Gamma^2m_1 - a^2k\Gamma_2^2m_1 - a^2kr\Gamma_1b_1m_1 - ak\Gamma_1b_1m_1^2 + ak\Gamma_1b_1m_1^2} \tag{11}$$

$+krb_1^2 m_1^2 + rm_1 a\Gamma_1 + rb_1 m_1^2 - 4a^4 k^2 r\Gamma_1^4 m_1$
$+a^4 k^2 \Gamma_1^4 m_1^2 - (2a^4 k^2 \Gamma_1^4 m_1^2 + a^4 k^2 \Gamma_1^4 m_1^2 + 2a^3 k^2 r\Gamma_1^3 b_1 m_1^2$
$+10a^3 k^2 r\Gamma_1^2 \Gamma_1 b_1 m_1^2 - 2a^3 k^2 \Gamma_1^3 b_1 m_1^3 + 4a^3 k^2 \Gamma_1^3 b_1 m_1^3 - 2a^3 k^2 \Gamma_1^3) b_1 m_1^3$
$a^2 k^2 r^2 \Gamma_1^2 b_1^2 m_1^2 - 4a^2 k^2 r\Gamma_1^2 b_1^2 m_1^3 - (8a^2 k^2 r\Gamma_1^2) b_1^2 m_1^3 + a^2 k^2 \Gamma_1^2 b_1^2 m_1^4$
$-(2a^2 k^2 \Gamma_1^2 b_1^2 m_1^4 + a^2 k^2 \Gamma_1^2 b_1^2 m_1^4 - 2ak^2 r^2 \Gamma_1 b_1^3 m_1^3 + 2ak^2 r\Gamma_1 b_1^3 m_1^4 + 2ak^2 r\Gamma_1 b_1^3 m_1^4$
$+k^2 r^2 b_1^4 m_1^4 - 2a^3 krr\Gamma_1^3 m_1^2 + 6a^3 krr\Gamma_1^2 \Gamma_1) m_1^2 - 2a^2 kr^2 \Gamma_1^2 b_1 m_1^2 - (8a^2 kr\Gamma_1^2 \Gamma_1 m_1^3$
$+2akr\Gamma_1 b_1^2 m_1^4 + 2akr\Gamma_1 b_1 m_1^4 + 2kr^2 b_1^3 m_1 + a2r^2 \Gamma_1^2 m_1^2 + 2ar^2 \Gamma_1 b_1 m_1 + r^2 b_1 m_1.$

$$\lambda_4 = -m_3 \tag{12}$$

The system exhibits an unstable saddle-focus because the four eigenvalues obtained have mixed signs. This equilibrium can alternatively be interpreted as a saddle-node or a bifurcation point. Two of the eigenvalues being negative real numbers indicate stability along two state-space directions, meaning that small deviations in those directions gradually return to equilibrium. The complex conjugate eigenvalues, one positive and one negative, produce focus-like dynamics, so trajectories in the vicinity of the equilibrium display spiraling motion.
Dynamics near the full equilibrium $E5$ are captured by Eq. (4).
The Jacobian matrix $J4 = (aij)4\times4$ appears in Section 4. Denote the roots of the characteristic polynomial of $J4$ as λi for i = 1, 2, 3, 4, given by:

$$\sum_{i=0}^{4} A_i \lambda^{4-i} = 0, \tag{13}$$

Here, Ai represent sequentially dependent parameters, with $A0$ set equal to 1.

$$A_1 = -a_{1,1} - a_{2,2} - a_{3,3} - a_{4,4}. \tag{14}$$

$$A_2 = a_{1,1}a_{2,2} + a_{1,1}a_{3,3} + a_{1,1}a_{4,4} - a_{1,2}a_{2,1} + a_{2,2}a_{3,3} + a_{2,2}a_{4,4} - a_{2,3}a_{3,2} - a_{2,4}a_{4,2} + a_{3,3}a_{4,4}. \tag{15}$$

$$\begin{aligned} A_3 = {} & -a_{1,1}a_{2,2}a_{3,3} - a_{1,1}a_{2,2}a_{4,4} + {}_{1,1}a_{2,3}a_{3,2} + a_{1,1}a_{2,4}a_{4,2} - a_{1,1}a_{3,3}a_{4,4} + a_{1,2}a_{2,1}a_{3,3} \\ & + a_{1,2}a_{2,1}a_{4,4} - a_{1,2}a_{2,4}a_{4,1} - a_{2,2}a_{3,3}a_{4,4} + a_{2,3}a_{3,2}a_{4,4} - a_{2,3}a_{3,4}a_{4,2} \\ & + a_{2,4}a_{3,3}a_{4,2}. \end{aligned} \tag{16}$$

$$\begin{aligned} A_4 = {} & a_{1,1}a_{2,2}a_{3,3}a_{4,4} - a_{1,1}a_{2,3}a_{3,2}a_{4,4} + a_{1,1}a_{2,3}a_{3,4}a_{4,2} - a_{1,1}a_{2,4}a_{3,3}a_{4,2} - a_{1,2}a_{2,1}a_{3,3}a_{4,4} \\ & - a_{1,2}a_{2,3}a_{3,4}a_{4,1} + a_{1,2}a_{2,4}a_{3,3}a_{4,1}. \end{aligned} \tag{17}$$

Using the Routh-Hurwitz approach, a Jacobian matrix has all eigenvalues with negative real parts if the determinants of all associated Hurwitz matrices are positive. This means that a given equilibrium E is locally asymptotically stable only when $A_1 > 0$, $A_3 > 0$, $A_1 A_2 > A_3$, and $A_3 > \sqrt{A_1(A_1 A_4 - A_2 A_3)}$, or equivalently $A_1 A_2 A_3 > A_3^2 + A_1^2 A_4$. In the present case, we have ${}_1 < 0$ and $A_3 < 0$. Observing the Jacobian entries $a_{1,2}$<0, $a_{2,1}$>0, $a_{2,3}$<0, $a_{3,2}$>0, $a_{3,3}$<0, and $a_{4,4}$<0 it can be concluded that $A_1 A_2 A_3 > A_3^2 + A_1^2 A_4$ till holds. Therefore, by applying the Routh-Hurwitz conditions, we can explicitly state the necessary and sufficient requirements for the positive equilibrium to maintain local asymptotic stability. For clarity, the following notation is introduced.

$$a_{1,1} > 0\ i.e.if\ \alpha > \frac{aG_e}{(1+b_1 E_e)} + \frac{aE_e I_e b_1}{(1+b_1 E_e)2}\left(\frac{k}{(1-2E_e)}\right)\ and\ a_{1,2} < 0\ i.e.if\ \frac{-aEe}{(1+b_1 E_e)} < 0\ and$$
$$a_{2,1} > 0\ i.e.\ b_1 < \frac{E_e}{(1+b_1 E_e)}\ and\ a_{2,3} < 0\ if\ \zeta < \frac{C_e - 1}{C_e}\ and\ a_{4,4} < 0.$$

Consequently, $E4$ is identified as an unstable equilibrium. Trajectories in its neighborhood exhibit spiraling motion, whose persistence depends on the real parts of the complex eigenvalues. Here, one complex eigenvalue has a positive real part, and the other a negative one, classifying this equilibrium as a "saddle-point focus."

The analysis identified five distinct equilibria. The full dynamical equilibrium is particularly important because it includes all populations with positive values, and it occurs at $E4$. This equilibrium reflects the system's 'nowcasting' capability and demonstrates how variations in bed occupancy across departments propagate throughout the system, affecting both upstream and downstream components ('forecasting'). Upstream refers to beds in discharge or mortuary units, while downstream refers to beds in active departments, often called level 3 beds.

We studied the equilibria of the system, labeled ($E1$, $E2$, $E3$, $E4$, $E5$), evaluating their viability under biologically relevant conditions. To guarantee that the model produces realistic (non-negative) results, all initial conditions are specified:

$$E(0), C(0), G(0), I(0)$$

and parameters:

$$r, K, a, \beta, \zeta, m_1, m_2, m_2, \omega$$

as non-negative values, consistent with their real-world meanings. The components appearing in the equations, for example:

$$\frac{aEC}{1 + b_1 E},$$

are formulated so that they stay non-negative under these assumptions. In addition, the mortality rates:

$$m_1 C, m_2 G, m_3 I,$$

The terms are scaled according to the population sizes, ensuring that no variable can drop below zero. Analysis of the Jacobian eigenvalues shows that the biologically relevant equilibrium $E5$ is locally stable. Corresponding numerical simulations confirm that every state variable remains non-negative throughout the system's progression. This verifies that the model produces biologically consistent solutions given the chosen parameter set.

Parameter values investigation

A core objective of modeling population dynamics is to uncover the primary factors controlling system behavior, enabling predictions of responses to changes in environmental parameters [20]. In the hospital bed framework represented by Eq. (1), parameters in the base analysis correspond to the actual number of daily patient admissions. In UK hospitals, high bed occupancy constrains the number of patients admitted over a 24-hour period, as it is limited by beds becoming available due to discharges and deaths.

Patients arriving at the emergency department (ED) are evaluated for severity. Those requiring admission are either sent to a general medical ward G or a Covid ward C, based on the median number of transfers from the ED to wards, denoted by Γ1 and Γ2. Admissions are targeted to occur within 4 hours (a), the standard 'time to admit.' Patients whose condition deteriorates in medical wards are escalated to ICU care, with the median number of daily ICU transfers over the prior week represented by ζ.

Daily ward-specific mortality reflects patient case mix, with m1, m2, and m3 representing deaths in the general ward, Covid ward, and ICU, respectively. The total bed availability is calculated as the sum of daily discharges and deaths (ω). Because of limits on physical beds and staff, the threshold for admissions may be adjusted to prevent overcapacity. Eq. (1) describes patient flow from the ED, where steady-state admissions are determined by outflows (discharges and deaths) in the absence of Covid.

The next section provides a definition of the exogenous (independent) parameter values:

Numerical simulation results

Time series and phase portraits

The purpose of this section is to support the analytical results by using experimental parameter values obtained from a clinical consultant with hospital expertise. For the simulations, we employed the 14 parameter values provided in **Table 2**, which are used to explore the model in Eq. (1). These values also guided the selection of initial conditions for the numerical experiments. Another important goal here is to verify the analytical outcomes

(Table 1) through computational simulations. The results reveal several notable characteristics of the system from a practical standpoint.

Table 2. Descriptions of the parameters and their corresponding units applied in the model presented in Eq. (1).

Parameter	Definition	Value / Range	Units
r	Daily admission rate (number of new patients arriving in the past 24 hours)	5	dimensionless
K	Hospital carrying capacity (total effective resource/bed capacity)	100 – 200	dimensionless
a	Transfer rate from Emergency Department (ED) to inpatient wards under low COVID pressure (inverse of average processing time)	4	$hours^{-1}$
ζ	Linear occupancy-to-ICU admission rate coefficient	0.2	dimensionless
ε	Model reduction switch parameter ($\varepsilon = 0$ reduces the full model to a special case; $\varepsilon = 1$ retains the full four-compartment model)	0 or 1	dimensionless
$\Gamma_{1,2}$	Patient flow (transfer) rates between ED and other hospital departments	4 – 5	$hours^{-1}$
β	Fixed daily discharge capacity (maximum number of patients that can be discharged per day)	5	dimensionless
$b_{1,2}$	Average bed occupancy duration (length of stay) in general wards	1.5 – 2	$days^{-1}$
$m_{1,2,3}$	Mortality rate across compartments	1.5	dimensionless
ω	Patient discharge rate from the hospital (recovery turnover rate)	3.5	dimensionless

Figure 2 illustrates the local stability of the system near the second equilibrium $E2$. In this scenario, both the Covid ward and the general medical ward have zero population, and the system reaches a stable state with all trajectories converging toward the equilibrium. The oscillatory patterns are driven by the second positive root of the quartic polynomial, which governs the stability of the clinically significant equilibrium $E4$. For the 24-hour simulation, these oscillations capture short-term periodic behavior, whereas in the 500-hour simulation, they continue over a much longer timescale, reflecting extended regulatory influences. Similarly, **Figure 6** shows oscillatory trajectories, highlighting their sensitivity to both the initial conditions and the system's parameters.

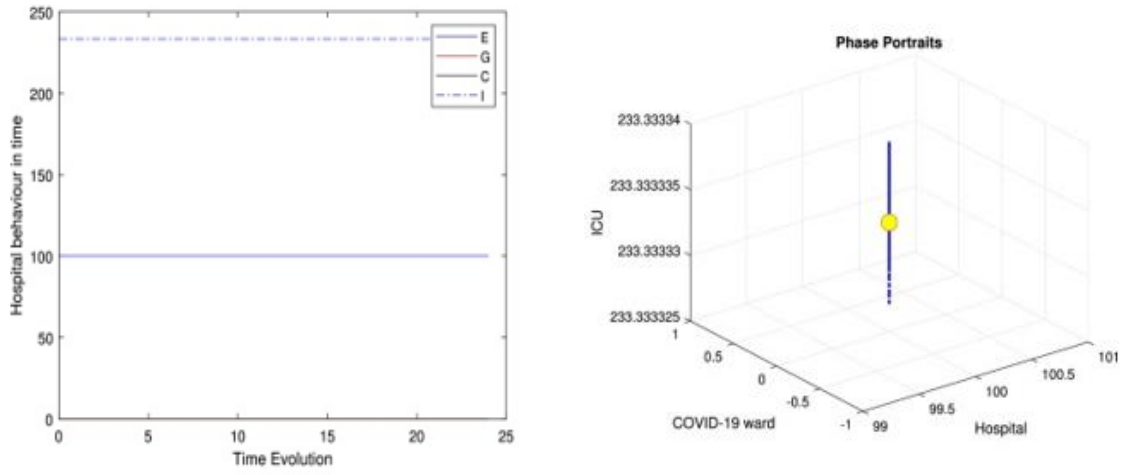

a) b)

Figure 2. shows the time series and phase portraits near the equilibrium point corresponding to hospital resources and the ICU equilibrium $E2$, given by (H_e,W_e,G_e,C_e)=(100,0,0,233.3333333) with $\zeta = 0.2$ and all other parameters fixed as in **Table 2**. The trajectories clearly converge to a stable limit cycle.

Figures 4 and 6 present the system's temporal evolution for the specific case model, with trajectories in HWC space under three distinct initial conditions: (He,We,Ge,Ce)=(0.2597,1.2983,0,0.49379), (0.15810,1.5440,7.6186,3.0031), and (99.9214,0.14818,4.5320,1565.697), using ζ=0.2 and all other parameters set to their default values. In **Figure**

4b, the trajectory converges onto a limit cycle with a period of roughly 500 hours, exhibiting substantial oscillations in H. These results reveal the system's inherent instability.

Prior analyses have mainly examined bed usage within individual departments (micro-level), rather than across the entire hospital system (macro-level). Here, we focus on bed utilization between departments within a hospital trust, which we term 'meso-activity.' **Figures 4-6** illustrate hospital activity over 24 hours, showing that nearly all departments operate under control with stable patient movement. Extending the simulation to 500 hours (approximately 20 days) highlights periodic dynamics, with trajectories forming a limit cycle around the three feasible, clinically relevant equilibria.

In the UK, emergency cases—including Covid patients—typically enter the hospital either after home assessment by a clinician (paramedic or occasionally GP) or by presenting at the ED. Triage is then conducted to assess the urgency of each patient, following a military-inspired classification: those likely to survive without intervention, those likely to die regardless, and those likely to survive only with intervention.

One-parameter bifurcation behavior

Numerical simulations of the model in Eq. (1) were used to investigate bifurcation behavior. **Figure 7** depicts the local stability diagram around $E4$ using the parameter values from **Table 2**. As shown in **Figure 7a**, if $E4<K$, the hospital population increases, while $E4>K$ signals resource shortages. Since $E4$ depends on ζ, the equilibrium is highly sensitive to bed numbers. If $E4=K$, the hospital population remains stable.

These simulations illustrate the $E–C–G–I$ clinical model. For specific parameters, the patient population can rise to very high levels yet eventually stabilize, while emergency population levels remain substantial. In real scenarios, stochastic fluctuations in patient admissions and life cycles may further increase population numbers, especially due to Covid and other conditions. Similarly, G and C populations can remain high, although chance variations in patient turnover may cause temporary decreases.

Heat map for hospital dynamics

To explore how variations in medical resources k affect population dynamics, we examined changes in k and ζ over 24 hours, presenting the results as a heat map in **Figure 7**. Cyclic system behavior from Eq. (1) shows that patient density rises in response to infection surges, and limited resources can increase mortality rates. Short-term dynamics in the general ward remain stable, supporting the assumption that resource constraints directly influence patient flow.

The heat map in **Figure 8** also highlights extreme responses in patient populations across wards due to variations in k and ζ, and illustrates how altered mortality affects equilibrium. Different levels of viral impact shape the stabilization of patient densities in each ward. Equilibria to the left of the curve in **Figure 8a** are unstable, while **Figure 8b** shows high densities in the E and C wards, indicated in red. Crossing the saddle-node curve produces an unstable equilibrium, demonstrating that increased patient flow places additional pressure on hospital resources and affects population densities in all wards.

Materials and Methods

This study was a cross-sectional study with the aim of comparing sexual satisfaction in women with and without Candida infection. The study was performed on 160 pregnant women referred to the specialized gynecology clinic, Shahid Beheshti Hospital, Tehran in 2019 in two groups of 80 patients with and without Candida. The inclusion criteria were no addiction, no history of neuropsychiatric illness, no medication affecting sexual function, no physical illness or surgery affecting sexual function, no severe marital conflict such as the threat of divorce and separation, and no pregnancy exclusion criteria. Non-participation were among the exclusion criteria.

After receiving the code of ethics and obtaining the necessary permits and coordinating with hospital authorities, the researcher attended various shifts (morning-evening) at the hospital's specialized clinic. Research units were selected by the researcher in terms of inclusion criteria, screening, and eligible individuals. Participants were fully informed about the purpose of the study, the confidentiality of the answers, and knowledge of the results of the study. After obtaining written informed consent, data collection was done in both groups, and the sampling method was random. Pregnant mothers with Candida infection were diagnosed by a specialist midwife with the genital examination and clinical symptoms. Unsuspecting pregnant individuals were mothers with none of the clinical signs and symptoms of Candida infection, such as itching, burning, etc. The data collection tool was a

questionnaire with two sections. The first section included personal information such as education level, occupation of the woman, and her spouse, body mass index, housing status, income, and pregnancy status. The second part of the questionnaire was the Larson Sexual Satisfaction Questionnaire that consisted of 25 items, 13 of which (25, 24, 20, 18, 15, 14, 11, 9, 8, 7, 6, 5, 4) were count reversed. The third part of the questionnaire was about the effect of antibiotics and corticosteroids on the sexual satisfaction of pregnant women infected with Candida. For this purpose, the Larson questionnaire was used to examine the effect of antibiotics and corticosteroids on sexual satisfaction in pregnant mothers who had used these drugs for three months. Answering questions is a Likert five-point (1 = never to 5 = always). The total score of this instrument is in between 25-125. 25-50 score of sexual dissatisfaction, 51-75 score of low sexual satisfaction, 76-100 score of moderate sexual satisfaction, and 101-125 score of high sexual satisfaction. This questionnaire was used in the study of Bahrami *et al*. (2016), with Cronbach's alpha coefficient of greater than 0.7. Its validity and reliability were determined for positive and negative questions, and it was determined that this questionnaire could be used in the Iranian population to measure sexual satisfaction. The research units in each group completed the Larsson Personal Information, and Sexual Satisfaction Questionnaires separately also the research units completed the questionnaires separately for privacy purposes. It took about 15 minutes to complete the questionnaires. After data collection, the data were analyzed by SPSS software and independent t-test. Finally, the relationship between the two concepts of sexual satisfaction and candidiasis in pregnant women was assessed.

Ethical considerations

Ethical considerations included providing information about the study, duration of the study, purpose, and type of study, obtaining informed written consent from pregnant mothers, ensuring the confidentiality of information, and being free to participate or not participating at any stage of the study.

Statistical analysis

Data were analyzed by SPSS software using an independent t-test. Frequency, percentage, mean, standard deviation, minimum, and maximum were determined using descriptive statistics. Independent t-test was used to compare sexual satisfaction scores between the two groups.

Results and Discussion

Since the pioneering work of Freedman [21, 22], Holling type II functional response models have been widely explored to better understand system dynamics and behaviours. More recent studies, including Freedman [23], focus on identifying periodic oscillations and assessing how the functional response shapes these dynamics [24]. In this study, we investigate the direction of trajectories by solving the model in Eq. (1). **Table 1** summarizes key analytical results, while additional numerical outcomes were generated using MATLAB's $O\times D\times E\times 45$ solver. The system in Eq. (1) presents four hyperbolic equilibria that are clinically relevant and one that is not feasible, $E3$. Equilibrium $E1$ corresponds to the extinction of all hospital populations and is consistently stable. Equilibrium $E2$ occurs when the ED is at maximum occupancy, while the Covid ward and general medical ward remain empty, and ICU occupancy is limited; this state is also stable. Equilibrium $E3$ is not clinically meaningful because it produces a negative population for at least one department. The clinically relevant equilibrium $E4$ is derived from a quartic polynomial with four real roots—two negative and three positive—all of which support surviving populations. Each positive root exhibits distinct dynamic behaviour.

The $E4$ equilibrium acts as a saddle-focus, combining stable and unstable components with oscillatory motion. Stability is governed by the real eigenvalues, whereas the complex conjugate eigenvalues drive the oscillations. **Figures 4a and 4b** display the general medical ward free equilibrium, while **Figures 4c and 4d** depict the first positive root of the quartic polynomial—clinically relevant $E4$—over 24-hour and 500-hour periods, as specified in Eq. (13), with all other parameters set according to **Table 2**.

The parameters in **Table 2** generate a variety of system behaviours even within a narrow range of ζ values. Stability patterns can be classified into four types based on population dynamics or limit-cycle behaviour [25]. An 'unstable spiral' emerges when trajectories diverge from initial conditions, producing unbounded oscillations. Our simulations reveal that this oscillatory region persists across the parameter ranges listed in **Table 2**, consistent with results in [22].

The oscillations in the hospital model primarily result from the ICU bed functional response (C), which plays a critical role in system dynamics and has clinical significance [22]. Prior work [26] shows that even a simple reaction-diffusion model can reproduce complex oscillatory dynamics by focusing on trophic interactions.
Interestingly, the limit-cycle behaviour observed with linear mortality functions for the Covid ward (W), general ward (G), and ICU (C) may disappear if quadratic mortality functions are applied to G and C. Numerical simulations using *ODE*45 confirm this. **Figure 2** presents the time series **(Figure 2a)** and phase portraits **(Figure 2b)** near the ICU and hospital resource equilibrium $E2$, with $\zeta = 0.2$ and all other parameters fixed as in **Table 2**, showing convergence onto a stable limit cycle. **Figure 3** illustrates the system near the general ward free equilibrium $E3$, with the same parameters, where trajectories converge to an unstable limit cycle, displaying oscillatory behaviour as shown in **Figures 3a and 3b**.

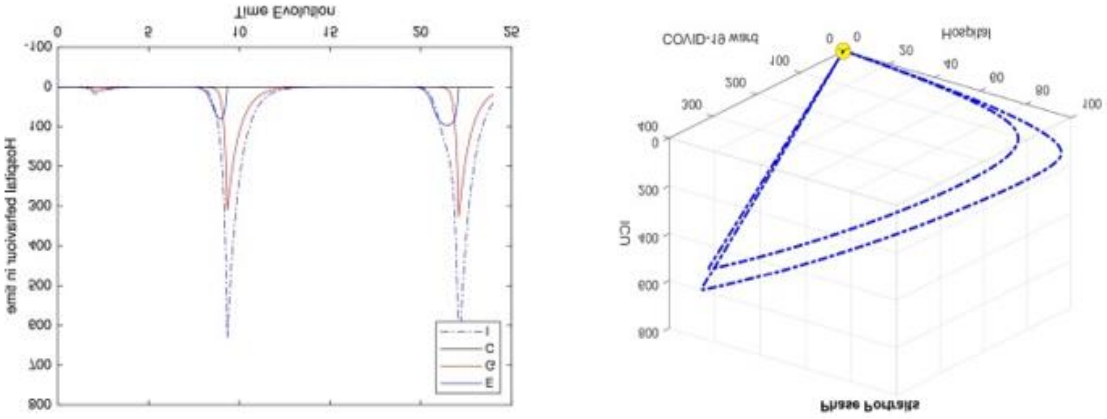

a) b)

Figure 3. shows the system's trajectories near the general ward free equilibrium $E3$, defined by (H_e,W_e,G_e,C_e)=(0.02597402597,1.298363974,0,0.4934840052) with $\zeta = 0.2$, while keeping all other parameters as listed in **Table 2**. In this configuration, the system evolves toward an unstable limit cycle, with clear oscillatory fluctuations observable in the time series and phase portraits.

The dynamics become more pronounced in **Figures 4a–4d**, where the clinically relevant equilibrium shows instability when $\zeta = 2.3$. Similarly, **Figures 5a–5d** illustrate the behaviour associated with the second positive root of the quartic polynomial, corresponding to equilibrium $E4$ over both 24-hour and 500-hour periods. **Figure 6** confirms analogous patterns, demonstrating persistent oscillatory dynamics and highlighting the unstable nature of this clinically significant state.

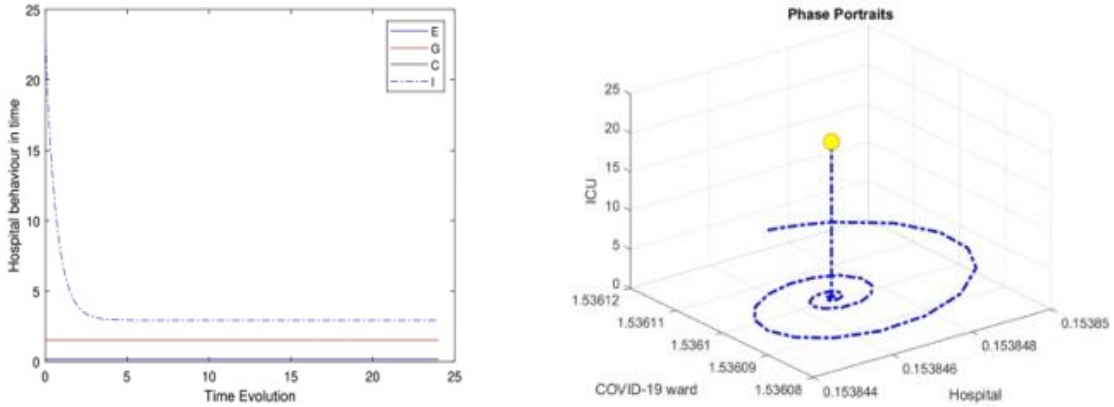

a) b)

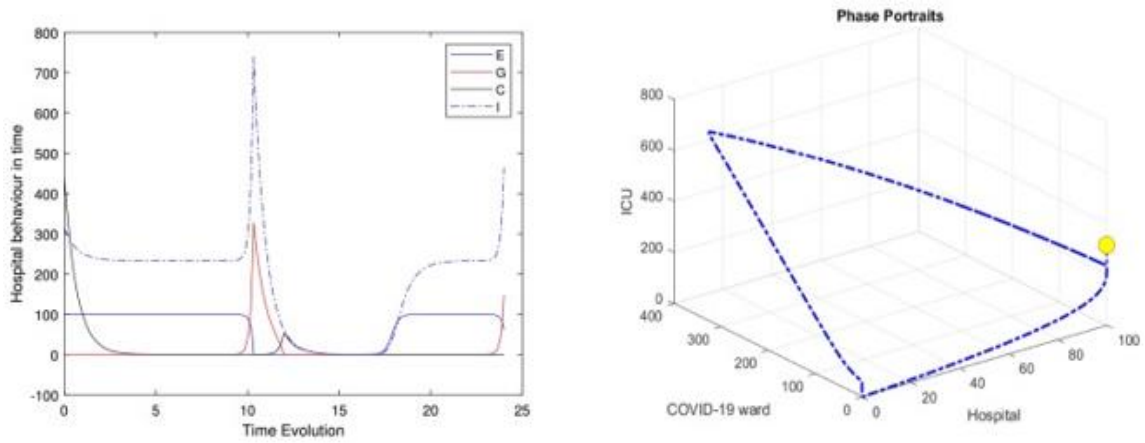

c) d)

Figure 4. presents the evolution of the system for the general medical ward free equilibrium. The time series and phase-space paths in panels 4(a) and 4(b) correspond to the chosen initial conditions for this equilibrium. Panels 4(c) and 4(d) display the behaviour associated with the first positive root of the quartic polynomial, representing the clinically significant equilibrium $E4$, over 24-hour and 500-hour simulations as specified in Eq. (13). All other parameters remain fixed according to the values in **Table 2**.

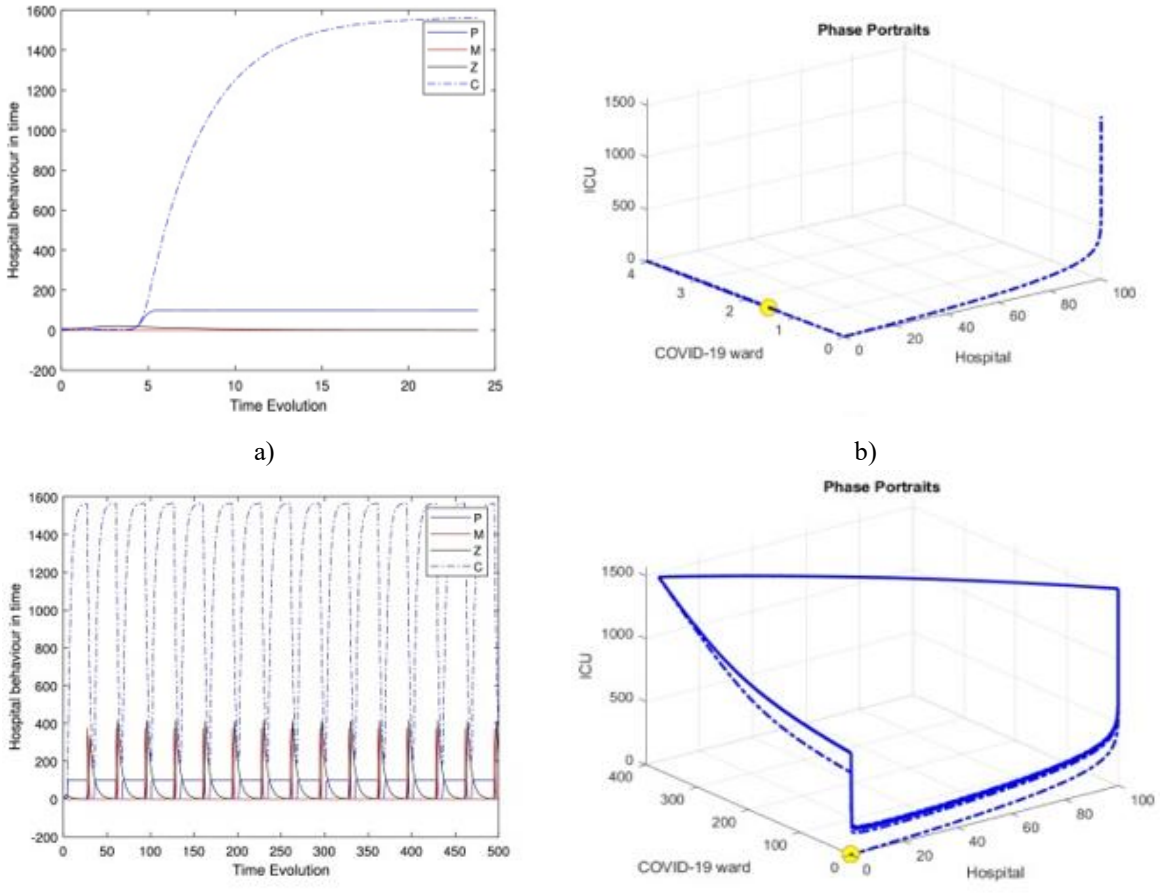

a) b)

c) d)

Figure 5. Time series and phase-space trajectories near the proposed initial condition for the second positive root of the quartic polynomial, corresponding to the clinically relevant equilibrium E_4, for durations of 24 hours and 500 hours. This equilibrium is defined in Eq. (13), with all other parameters maintained as specified in **Table 2**.

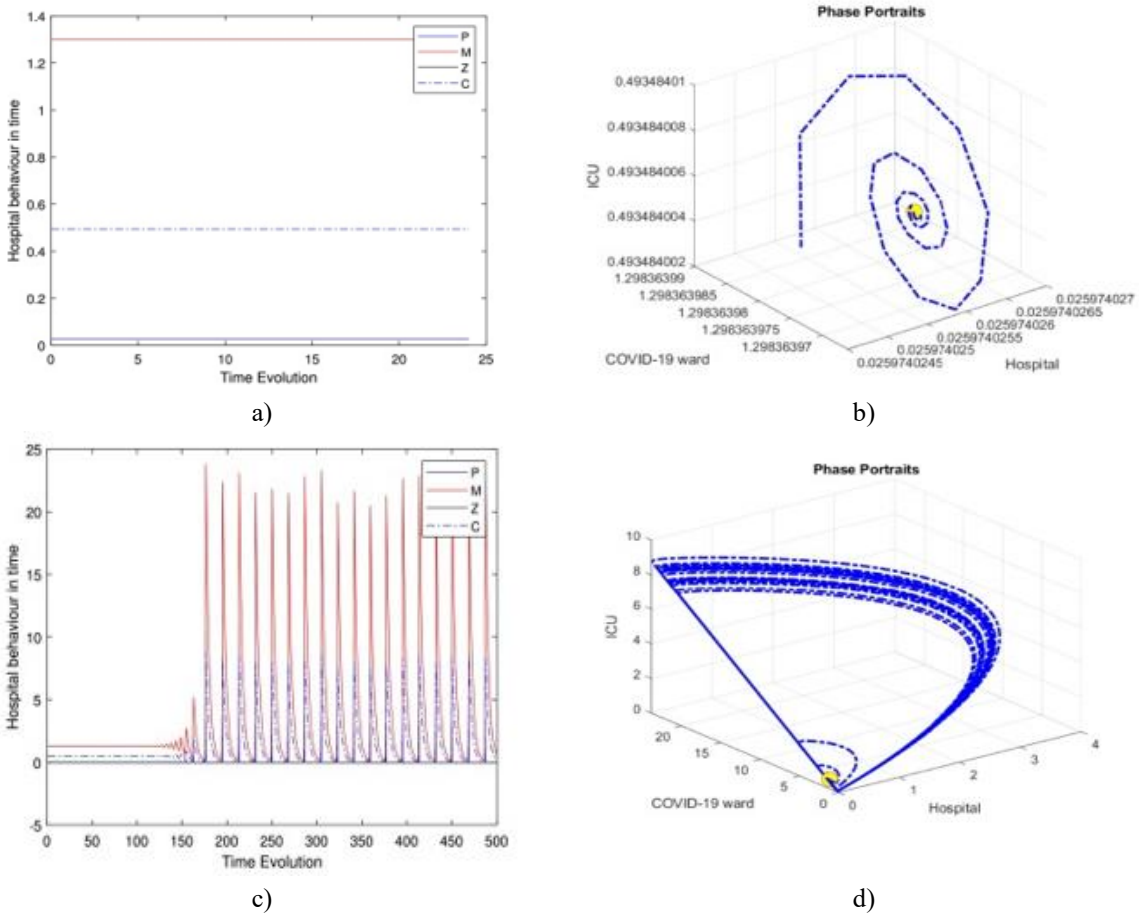

Figure 6. Time series and phase-space trajectories near the proposed initial condition for the third positive root of the quartic polynomial, representing the clinically relevant equilibrium E_4 over 24-hour and 500-hour intervals. Eq. (13) defines this equilibrium, and all other parameters remain as in **Table 2**.

The model described by Eq. (1) shows an unstable region in the vicinity of Hopf bifurcations for the parameter set K=20, r=4.455, ζ=2.3, and ω=1.5. Nevertheless, it does not reproduce dynamics consistent with the enrichment paradox. Increasing the hospital's core resources K drives the system through unstable states; however, larger populations in both W and C maintain instability at higher K values. This behavior provides detailed insight into the interplay among the three hospital departments.

Conclusion

The main objective of this work is to deepen the understanding of hospital dynamics as described by Eq. (1). The study confirms the presence of periodic oscillations in the system and assesses how viral dynamics influence hospital operation. It emphasizes the importance of comprehending COVID-19 transmission effects within hospital ward structures. Trajectories were analyzed by solving Eq. (1), and **Table 1** summarizes the numerical outcomes obtained using MATLAB's ODE45 solver. The model identifies four hyperbolic, clinically feasible equilibria along with a single non-viable equilibrium, $E3$. The first equilibrium, $E1$, represents complete population extinction (empty hospital) and is always unstable. This analysis aims to enhance understanding of hospital dynamics during the COVID-19 pandemic under limited bed capacity conditions. Equilibrium $E2$ occurs when patients in E are maximized while C and G populations vanish, constraining COVID-19 spread, which renders it unstable (Section 4). Equilibrium $E3$ corresponds to persistent patient presence and virus spread despite depletion of hospital resources. The fourth equilibrium, $E4$, reflects coexistence where all ward populations are present, as detailed in Section 3.

Parameter choices from **Table 2** allow observation of diverse behaviors within a narrow ζ range. System stability can be categorized into four classes based on $E{-}C{-}G{-}I$ population dynamics or limit-cycle behavior [25]. An unstable spiral emerges from the initial conditions, producing unbounded population oscillations. This oscillatory

region is demonstrated in the four-species model and persists under the parameter set in **Table 2**. Oscillations in the $E{-}C{-}G{-}I$ model highlight the challenges of using Holling type II functional responses in clinical settings, as they capture realistic saturation effects: patient transfer rates slow as ward capacity is approached. If quadratic mortality functions replace linear ones, observed limit-cycle behavior may not occur [24].

Numerical results in **Figure 7**, computed via ODE45 for various equilibria, show that the coexistence equilibrium becomes unstable when ζ=0.001. Here, a neutral center manifests as a closed loop with undamped oscillations. A stable spiral slowly converges to equilibrium, with population oscillations gradually decreasing until stability is reached. These findings will be validated using actual hospital patient flow data.

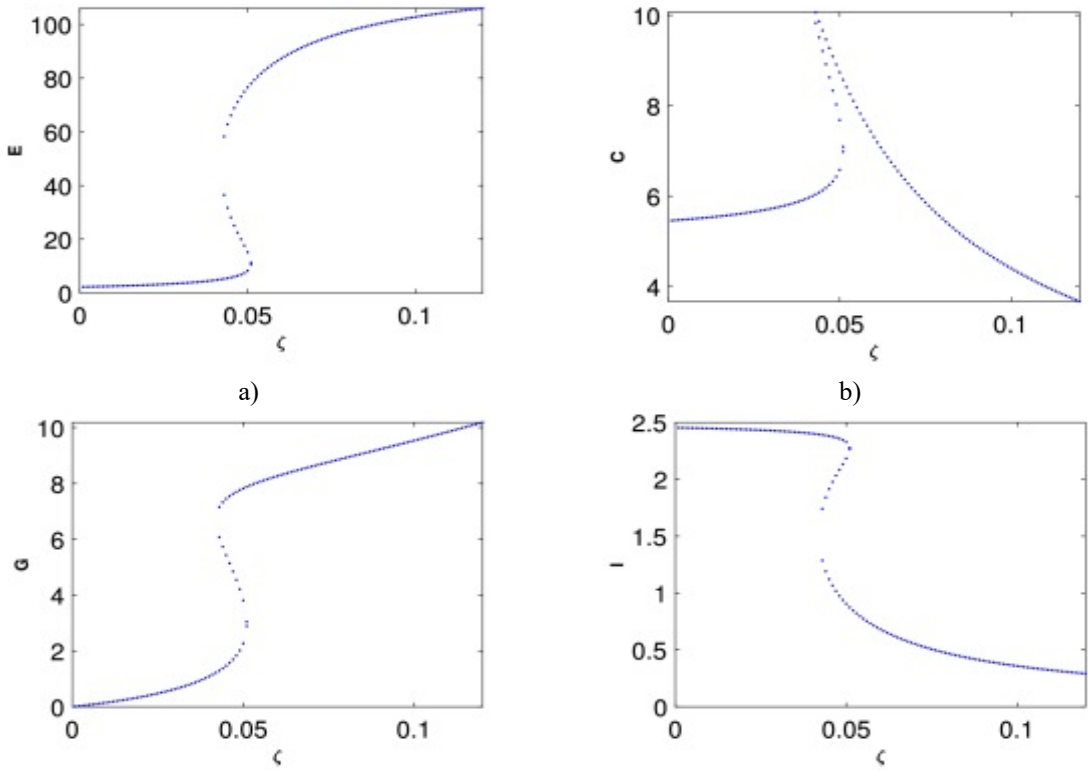

Figure 7. Clinically significant equilibrium with respect to ζ, considered as the hospital bed capacity parameter.

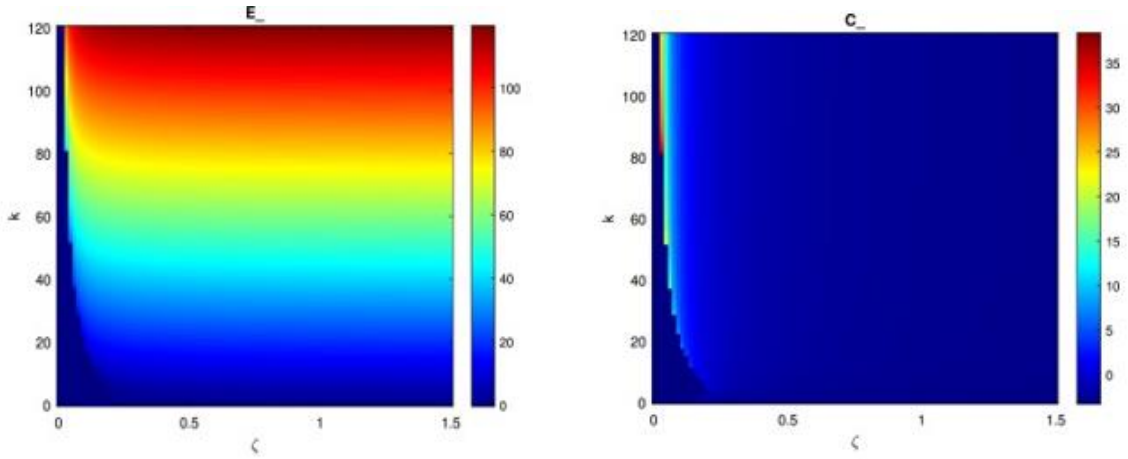

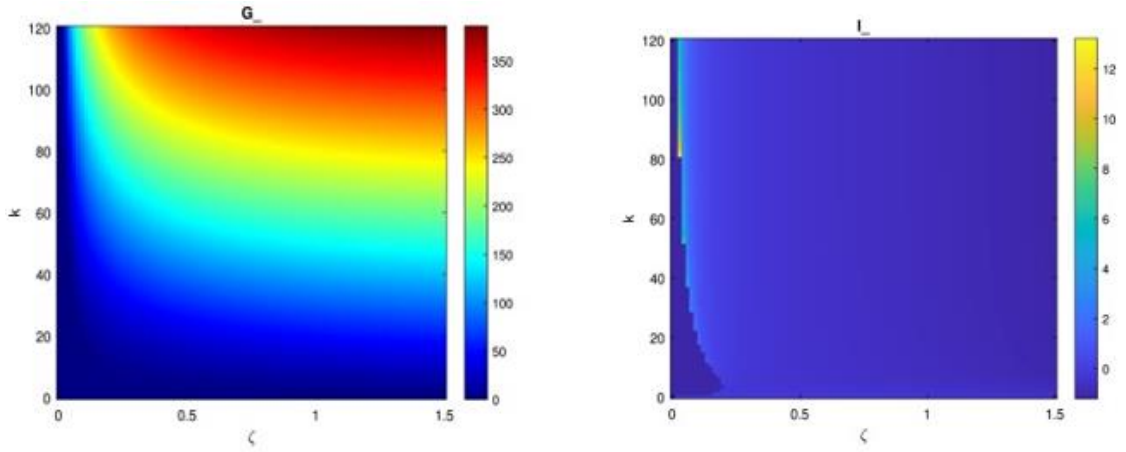

c) d)

Figure 8. Heat map illustrating hospital dynamics and stability over a 24-hour period, showing the system's maximum equilibrium (E_e,C_e,G_e,I_e) for varying values of K and ζ. **Figure 8a** displays the heat map for the emergency department EEE, highlighting sustained high population levels, indicated by the red coloration. **Figure 8d** depicts the ICU, where the population remains low due to limited bed availability.

Acknowledgments: We would like to thank Professor Christian Ghiglion and the School of Mathematics, Statistics and Actuarial Science at the University of Essex for their support and encouragement in this project.

Conflict of Interest: None

Financial Support: None

Ethics Statement: None

References

1. Anon, Health at a glance 2023: OECD indicators, https://www.oecd.org/en/publications/2023/11/health-at-a-glance-2023_e04f8239.html, 2023. (Accessed 12 November 2024).
2. Anon, Hospital bed occupancy, https://www.nuffieldtrust.org.uk/resource/hospital-bed-occupancy/, 2024. (Accessed 11 November 2024).
3. John H. Milsum, Efraim Turban, Ilan Vertinsky, Hospital admission systems: their evaluation and management, Manag. Sci. 19 (6) (1973) 646–666.
4. Robert Schmidt, Sandra Geisler, Cord Spreckelsen, Decision support for hospital bed management using adaptable individual length of stay estimations and shared resources, BMC Med. Inform. Decis. Mak. 13 (1) (2013) 1–19.
5. René Bekker, Paulien M. Koeleman, Scheduling admissions and reducing variability in bed demand, Health Care Manage. Sci. 14 (2011) 237–249.
6. Christina Pagel, Victoria Banks, Catherine Pope, Pauline Whitmore, Katherine Brown, Allan Goldman, Martin Utley, Development, implementation and evaluation of a tool for forecasting short term demand for beds in an intensive care unit, Oper. Res. Health Care 15 (2017) 19–31.
7. Huiyin Ouyang, Nilay Tanık Argon, Serhan Ziya, Allocation of intensive care unit beds in periods of high demand, Oper. Res. 68 (2) (2020) 591–608.
8. Syed Mohiuddin, John Busby, Jelena Savović, Alison Richards, Kate Northstone, William Hollingworth, Jenny L. Donovan, Christos Vasilakis, Patient flow within UK emergency departments: a systematic review of the use of computer simulation modelling methods, BMJ Open 7 (5) (2017).
9. Smaranda Belciug, Florin Gorunescu, A hybrid genetic algorithm-queuing multi-compartment model for optimizing inpatient bed occupancy and associated costs, Artif. Intell. Med. 68 (2016) 59–69.

10. Peter H. Millard, Georgina Christodoulou, Carol Jagger, Gary W. Harrison, Sally I. McClean, Modelling hospital and social care bed occupancy and use by elderly people in an English health district, Health Care Manage. Sci. 4 (2001) 57–62.
11. Anders Reenberg Andersen, Bo Friis Nielsen, Line Blander Reinhardt, Optimization of hospital ward resources with patient relocation using Markov chain modeling, Eur. J. Oper. Res. 260 (3) (2017) 1152–1163.
12. Ekaterina Kutafina, Istvan Bechtold, Klaus Kabino, Stephan M. Jonas, Recursive neural networks in hospital bed occupancy forecasting, BMC Med. Inform. Decis. Mak. 19 (2019) 1–10.
13. Seyede Maryam Najibi, Seyed Hosein Seyedi, Payam Farhadi, Erfan Kharazmi, Payam Shojaei, Sajad Delavari, Farhad Lotfi, Zahra Kavosi, Development of a model for predicting hospital beds shortage and optimal policies using system dynamics approach, BMC Health Serv. Res. 22 (1) (2022) 1525.
14. Sally C. Brailsford, Valerie A. Lattimer, P. Tarnaras, J.C. Turnbull, Emergency and on-demand health care: modelling a large complex system, J. Oper. Res. Soc. 55 (2004) 34–42.
15. Priyantha Devapriya, Christopher T.B. Strömblad, Matthew D. Bailey, Seth Frazier, John Bulger, Sharon T. Kemberling, Kenneth E. Wood, Stratbam: a discrete- event simulation model to support strategic hospital bed capacity decisions, J. Med. Syst. 39 (2015) 1–13.
16. Michael G. Klein, Carolynn J. Cheng, Evonne Lii, Keying Mao, Hamza Mesbahi, Tianjie Zhu, John A. Muckstadt, Nathaniel Hupert, COVID-19 models for hospital surge capacity planning: a systematic review, Disaster Med. Public Health Prep. 16 (1) (2022) 390–397.
17. Mieke Deschepper, Kristof Eeckloo, Simon Malfait, Dominique Benoit, Steven Callens, Stijn Vansteelandt, Prediction of hospital bed capacity during the COVID-19 pandemic, BMC Health Serv. Res. 21 (1) (2021) 468.
18. Fabrizio Pecoraro, Daniela Luzi, Fabrizio Clemente, The efficiency in the ordinary hospital bed management: a comparative analysis in four European countries before the COVID-19 outbreak, PLoS ONE 16 (3) (2021) e0248867.
19. A.K. Misra, Jyoti Maurya, Mohammad Sajid, Modeling the effect of time delay in the increment of number of hospital beds to control an infectious disease, Math. Biosci. Eng. 19 (11) (2022) 11628–11656.
20. J.D. Murray, Mathematical Biology I: An Introduction, Interdisciplinary Applied Mathematics, vol. 17, Springer, New York, NY, USA, 2002.
21. Robert McCredie May, Stability and Complexity in Model Ecosystems, vol. 6, Princeton University Press, 1973.
22. Andrew M. Edwards, John Brindley, Oscillatory behaviour in a three-component plankton population model, Dyn. Stab. Syst. 11 (4) (1996) 347–370.
23. H.I. Freedman, R.M. Mathsen, Persistence in predator-prey systems with ratio-dependent predator influence, Bull. Math. Biol. 55 (4) (1993) 817–827.
24. Tahani A.S. Al-Karkhi, The stability analysis of the plankton full interaction model, in: AIP Conference Proceedings, vol. 2554, AIP Publishing, 2023.
25. H.I. Freedman, Paul Waltman, Persistence in models of three interacting predator-prey populations, Math. Biosci. 68 (2) (1984) 213–231.
26. Muniyagounder Sambath, Krishnan Balachandran, Murugan Suvinthra, Stability and Hopf bifurcation of a diffusive predator-prey model with hyperbolic mor- tality, Complexity 21 (S1) (2016) 34–43.